remote sensing

MDPI

Article

Spatiotemporal Patterns and Driving Factors of Carbon Emissions from Forest Fires in Heilongjiang Province, China (2001–2022)

Yushan Jiang †, Huiying Cai †, Honglin Xiang, Lin Liu and Long Sun *

College of Forestry, Northeast Forestry University, Harbin 150040, China; jiang2020223816@nefu.edu.cn (Y.J.); caihy0606@nefu.edu.cn (H.C.); xianghonglin@nefu.edu.cn (H.X.); liulin2018@nefu.edu.cn (L.L.)
* Correspondence: sunl-cf@nefu.edu.cn
† These authors contributed equally to this work.

Highlights

What are the main findings?

- From 2001 to 2022, forest fire carbon emissions in Heilongjiang Province showed significant overall downward trends and a distinct spatial pattern characterized by higher emissions in the north and lower emissions in the south, with significant spatial clustering.
- The GTWR model revealed pronounced spatiotemporal heterogeneity in the associations between driving factors and forest fire CO_2 emissions. Fractional vegetation cover showed a relatively strong association with forest fire CO_2 emissions.

What are the implications of the main findings?

- Forest fire carbon emission estimates should adequately account for key parameters such as burned area and combustion efficiency, as well as their associated uncertainties.
- The findings reveal the spatiotemporal patterns of regional forest fire carbon emissions and their driving factors, providing scientific references for targeted forest fire prevention and management.

Abstract

Forest fires are an important disturbance to the carbon cycle of terrestrial ecosystems and a major source of regional carbon emissions. This study used the emission factor method to estimate forest fire CO_2, CO, and CH_4 emissions in Heilongjiang Province from 2001 to 2022. The geographically and temporally weighted regression (GTWR) model was applied to examine spatiotemporal heterogeneity in the relationships between driving factors and CO_2 emissions. Cumulative CO_2, CO, and CH_4 emissions were 72.95 Tg, 5171.73 Gg, and 246.54 Gg, respectively. Mean emissions per hectare of burned forest were 32.02, 2.27, and 0.108 Mg ha^{-1} for CO_2, CO, and CH_4, respectively. Emissions of all three gases showed significant downward trends ($p < 0.001$) and a bimodal monthly pattern with spring and autumn peaks. Deciduous broadleaf forests contributed 95.6% of CO_2 emissions. Spatially, CO_2 emissions were higher in the north than in the south and exhibited significant spatial clustering. The GTWR model achieved an adjusted R^2 of 0.585, and fractional vegetation cover was the main influencing factor among the variables examined. Forest fire carbon emission estimates remain subject to some uncertainty. The results provide scientific support for regional forest fire risk management and forest fire carbon emission mitigation.

Keywords: forest fire; CO_2 emission; burned area fusion; dNBR; emission factor method; GTWR

Check for updates

Academic Editor: Nikolay S. Strigul

Received: 27 September 2026
Revised: 7 November 2026
Accepted: 11 November 2026
Published: 13 November 2026

Copyright: © 2026 by the authors. Licensee MDPI, Basel, Switzerland. This article is an open access article distributed under the terms and conditions of the Creative Commons Attribution (CC BY) license.

1. Introduction

As one of the major disturbance factors in forest ecosystems, forest fires can cause tree mortality and the loss of forest carbon stocks, thereby weakening the carbon sequestration capacity of forest ecosystems [1]. Meanwhile, the combustion process of forest fires releases substantial amounts of greenhouse gases, exerting important influences on regional and global carbon cycles and carbon balances [2,3]. Although the global burned area has generally exhibited a declining trend since the beginning of the 21st century, CO_2 emissions from forest fires have continued to increase at an annual rate of approximately 1% (about 15 million tonnes), driven by the combined effects of climate warming and human activities, making forest fires an increasingly important source of carbon emissions [4]. Notably, carbon emissions from boreal forest fires increased markedly in 2021, accounting for 23% of global wildfire carbon emissions and reaching a total of 1.76 billion tonnes of CO_2, substantially exceeding the long-term average level [5]. This highlights boreal forest regions as one of the major source areas of global carbon emissions from forest fires. As an important concentration area of forest resources in northern China, Heilongjiang Province experiences relatively frequent forest fire activities and provides a representative case for studying carbon emissions from forest fires.

Methods for calculating carbon emissions from wildfires primarily fall into two categories: "top-down" and "bottom-up." The "top-down" approach primarily uses atmospheric observation data and atmospheric chemical transport models to estimate fire emissions through inversion. Byrne et al. [6] estimated carbon emissions from forest fires in Canada in 2023 using the CMS-Flux inversion system based on TROPOMI carbon monoxide observations and multiple fire emission inventories. In contrast, the "bottom-up" approach primarily estimates greenhouse gas emissions from fuel consumed by fire using burned area or fire radiative power (FRP), together with parameters such as biomass, combustion efficiency, and emission factors [7]. Among these approaches, the emission factor method is a typical "bottom-up" approach and is widely used to estimate carbon emissions from forest fires at regional and global scales because of its clear computational framework and relatively low data requirements [8]. The theoretical basis of this method originates from the biomass-loss model for forest fires proposed by Seiler and Crutzen [9]. Hu et al. [10–12] combined forest resource inventory data, forest fire statistics, and GIS techniques, and employed the emission factor method based on field surveys of burned areas and laboratory-controlled experiments to estimate carbon emissions from forest fires in the Greater Khingan Mountains from 1965 to 2010 and from 2001 to 2010, as well as in the Lesser Khingan Mountains from 1953 to 2011. With the advancement of remote sensing technologies, multi-source remote sensing data have increasingly been used for the retrieval and spatially explicit estimation of key parameters for forest fire carbon emission estimation. Liu and Shi [2] used active fire data from the FY-3 satellite series, together with multi-source remote sensing information such as NDVI and land-cover data, to estimate fuel loads and dynamically calculate combustion factors, and subsequently used the emission factor method to estimate global carbon emissions from forest fires from 2016 to 2022. Overall, a relatively mature framework for estimating carbon emissions from forest fires has been established. However, several limitations remain. First, most studies rely on a single burned area product, and differences among products in spatial resolution and burned-area detection capability may introduce biases in burned area estimates, thereby affecting carbon emission estimates [13]. Second, combustion efficiency is often assigned fixed empirical values, making it difficult to capture its dynamic variation under different burn severity conditions [14].

Building on the estimation of carbon emissions from forest fires, researchers have conducted extensive studies on their spatiotemporal patterns and driving factors. Zhang et al. [15] found that carbon emissions from forest fires in China from 1988 to 2012 exhibited pro-

nounced interannual fluctuations and spatial heterogeneity, with high-emission areas mainly concentrated in North China and Northeast China. Based on the Global Fire Emissions Database (GFED), van der Werf et al. [16] reported substantial differences in fire carbon emission contributions among ecosystems, with boreal and tropical forests representing major sources of global fire carbon emissions. Regarding the driving factors of carbon emissions from forest fires, Guo et al. [17] employed the Geographical Detector method and found that meteorological factors, including temperature, precipitation, and relative humidity, as well as their interactions, exhibited strong explanatory power for the spatial distribution of forest fire CO_2 emissions, indicating that meteorological conditions are important drivers of carbon emissions from forest fires. Gong et al. [18] employed a Geographically and Temporally Weighted Regression (GTWR) model and found that factors such as air temperature, relative humidity, and GDP significantly affected forest fire CO_2 emissions. However, both the direction and magnitude of these effects varied considerably across regions and over time. Nevertheless, systematic studies on the driving factors of carbon emissions from forest fires in key forest regions of northern China over long-term periods remain limited.

Heilongjiang Province is one of China's major forestry provinces and contains major state-owned forest areas in the Greater Khingan Mountains and Lesser Khingan Mountains. It possesses abundant forest resources and substantial carbon stocks. At the same time, Heilongjiang Province is one of the forest fire-prone regions in China [19]. Frequent forest fires not only threaten regional ecological security but also increase regional carbon emissions. To date, systematic studies on the long-term spatiotemporal patterns and driving factors of carbon emissions from forest fires in Heilongjiang Province remain limited. To address this research gap, this study focuses on Heilongjiang Province and conducts a long-term assessment of forest fire carbon emissions from 2001 to 2022. Two burned area products (FireCCI51 and MCD64A1) were integrated using a rule-based fusion approach to reduce reliance on a single burned area product and retain non-overlapping burned-area information. The differenced Normalized Burn Ratio (dNBR) was introduced to characterize burn severity and to estimate combustion efficiency as a function of dNBR, rather than assigning a fixed empirical value. The emission factor method was then employed to estimate CO_2, CO, and CH_4 emissions from forest fires, and the GTWR model was applied to characterize the spatiotemporal heterogeneity of the relationships between different driving factors and forest fire CO_2 emissions. This study contributes by incorporating remotely sensed burn severity into a long-term assessment of forest fire carbon emissions and examining the effects of natural and human activity factors on forest fire CO_2 emissions in Heilongjiang Province and their spatiotemporal variation, providing a reference for regional-scale assessments of forest fire carbon emissions and investigations of their driving factors. The objectives of this study are as follows: (1) to reveal the spatiotemporal patterns and spatial clustering characteristics of carbon emissions from forest fires; (2) to identify the driving factors of forest fire CO_2 emissions and their spatiotemporal heterogeneity. The findings may inform regional assessments of forest fire carbon emissions and the development of targeted forest fire prevention and control strategies.

2. Materials and Methods

2.1. Study Area

Heilongjiang Province is located in northeastern China (43°26′–53°33′N, 121°11′–135°05′E) and covers a land area of approximately 473,000 km^2 (Figure 1). It shares river boundaries with Russia to the north and east, borders the Inner Mongolia Autonomous Region to the west, and adjoins Jilin Province to the south. The region exhibits diverse topography, consisting mainly of mountains, hills, and plains. Major mountain ranges include the Greater

Khingan Mountains, the Lesser Khingan Mountains, the Zhangguangcai Mountains, and the Wanda Mountains, with elevations typically ranging from 400 to 1200 m. Areas such as the Songnen Plain and the Sanjiang Plain mostly lie below 200 m above sea level. The region is characterized by a mid-temperate to cold-temperate continental monsoon climate, with long, cold winters and short, warm summers. The mean annual temperature ranges from approximately −5 to 5 °C, while annual precipitation ranges from about 500 to 600 mm, most of which occurs during summer. Spring and autumn are typically dry and windy, resulting in elevated forest fire danger.

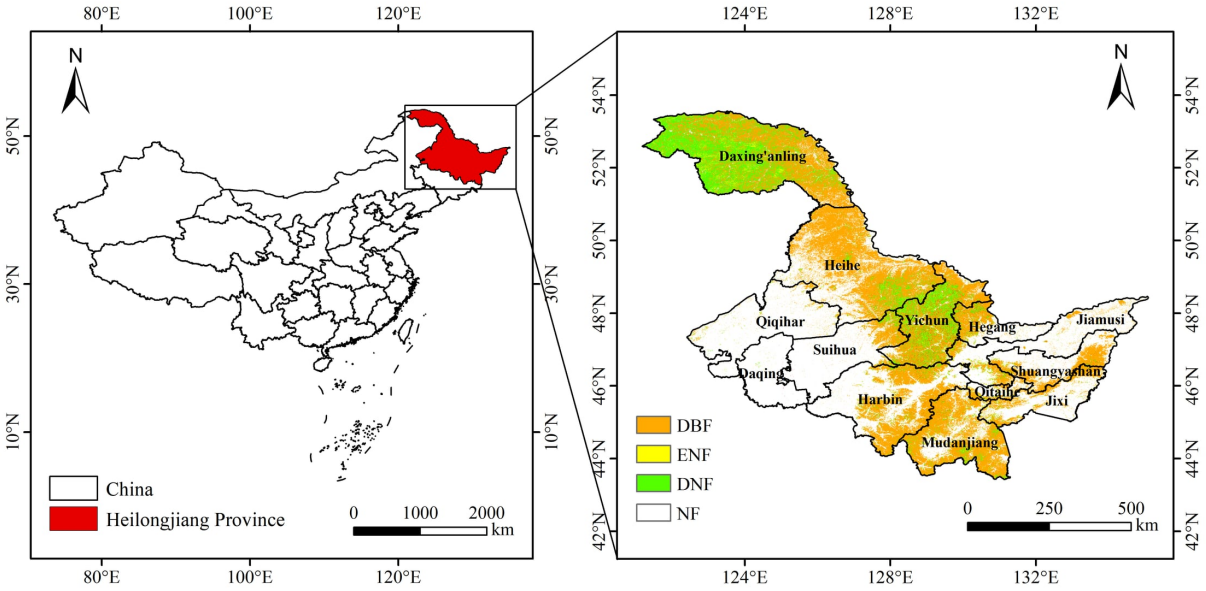


Figure 1. Location of the study area and distribution of forest types in 2022. Forest types were derived from GLC_FCS30D. DBF, Deciduous Broadleaf Forest; ENF, Evergreen Needleleaf Forest; DNF, Deciduous Needleleaf Forest; NF, Non-forest.

Heilongjiang Province is rich in forest resources and is one of China's major state-owned forest regions. Forests are mainly distributed in the Greater Khingan Mountains, the Lesser Khingan Mountains, and the eastern mountainous regions. Based on the 2022 GLC_FCS30D land-cover data, forests in the study area comprised evergreen broadleaf forest (EBF), deciduous broadleaf forest (DBF), evergreen needleleaf forest (ENF), deciduous needleleaf forest (DNF), and mixed forest (MF), accounting for 0.85%, 75.03%, 2.70%, 21.40%, and 0.01% of the total forest area, respectively. DBF was the predominant forest type, whereas EBF and MF accounted for relatively small proportions. Spatial overlays of forest-cover and burned-area data identified no burned pixels classified as EBF or MF during the study period. Therefore, subsequent forest fire emission estimates involved only DBF, ENF, and DNF.

2.2. Forest Fire Carbon Emission Estimation

Based on the biomass loss quantification model for forest fires proposed by Seiler and Crutzen [9], this study used the emission factor method to estimate CO_2, CO, and CH_4 emissions from forest fires in Heilongjiang Province from 2001 to 2022, while optimizing key parameters such as burned area and combustion efficiency. The emission estimation equation is as follows:

$$E_{i,j} = 10^{-3} \sum BA_j \times FL_j \times CF_j \times EF_{i,j} \quad (1)$$

where i and j represent the gas species and forest cover type, respectively. $E_{i,j}$ is the gas emission (Mg); BA_j is the burned area (ha); FL_j is the aboveground biomass density

($Mg \cdot ha^{-1}$); CF_j is the combustion efficiency (dimensionless); and $EF_{i,j}$ is the emission factor ($g \cdot kg^{-1}$). The CF_j values were estimated based on burn severity, which was characterized by the differenced Normalized Burn Ratio (dNBR). Burn severity was used only to determine combustion efficiency and was not applied as an independent parameter in Equation (1). The 10^{-3} term in the equation is a unit-conversion factor used to convert the calculated emissions to Mg. The parameters were spatially matched for emission estimation at a common 30-m grid to ensure consistency in spatial scale. This study used the monthly scale as the basic temporal unit for emission estimation and further aggregated the results to annual emissions for the analysis of interannual variation characteristics.

To characterize burn severity and estimate combustion efficiency, multi-temporal satellite imagery from the Landsat program at a spatial resolution of 30 m was processed and analyzed on the Google Earth Engine (GEE) platform (Google LLC, Mountain View, CA, USA). The Normalized Burn Ratio (NBR) was calculated separately from pre-fire and post-fire satellite imagery using the following equation:

$$\mathrm{NBR} = \frac{\rho_{\mathrm{NIR}} - \rho_{\mathrm{SWIR}}}{\rho_{\mathrm{NIR}} + \rho_{\mathrm{SWIR}}} \quad (2)$$

where ρ_{NIR} is the near-infrared reflectance and ρ_{SWIR} is the shortwave infrared reflectance.

The dNBR value was then derived from the difference between the pre-fire and post-fire NBR values according to the following equation:

$$\mathrm{dNBR} = \mathrm{NBR}_{\mathrm{pre}} - \mathrm{NBR}_{\mathrm{post}} \quad (3)$$

where $\mathrm{NBR}_{\mathrm{pre}}$ is the NBR value derived from the pre-fire imagery, and $\mathrm{NBR}_{\mathrm{post}}$ is the NBR value derived from the post-fire imagery.

A dNBR value of 0.2 was adopted as the threshold for burned-area delineation in this study [20]. The dNBR values within the delineated burned areas were used to estimate combustion efficiency for different forest types based on the regression relationships between dNBR and combustion efficiency established by Balde et al. [21]. When dNBR < 1, combustion efficiency for coniferous forests and broadleaf forests was estimated using Equations (4) and (5), respectively:

$$CF = e^{1.029\ \mathrm{dNBR} - 1.052} \quad (4)$$

$$CF = e^{1.669\ \mathrm{dNBR} - 1.618} \quad (5)$$

Spatially continuous combustion efficiency raster data were generated based on the above regression relationships. Finally, the estimated emissions were compared with Version 5.1 of the Global Fire Emissions Database (GFED5.1).

2.2.1. Fusion of Burned Area Datasets

During the data preprocessing stage, the two burned area datasets (FireCCI51 and MCD64A1) were clipped to the study area and reprojected to a common coordinate system. Since FireCCI51 and MCD64A1 provide burned area information in the form of burned pixels, burned areas were calculated using raster geometry-based methods. The processed burned area data were represented as polygon features containing information on burn perimeters and burned areas. To obtain a burned area dataset with both high spatial resolution and long temporal coverage, a rule-based fusion approach was employed to integrate the two datasets, with priority given to the product with higher spatial resolution during the fusion process. First, the low-resolution MCD64A1 (500 m) polygon dataset was converted into point features and spatially overlaid with the high-resolution FireCCI51 (250 m) polygon dataset for the corresponding year and month. When a low-resolution

point feature fell within a high-resolution burned-area polygon, the corresponding low-resolution feature was removed. The retained low-resolution polygon features were then merged with the high-resolution burned-area polygons to generate the final burned area dataset for the period from 2001 to 2022. To quantitatively assess the consistency of the fused burned area with the two input products, Spearman rank correlation analysis was performed. The fused results showed correlation coefficients of $\rho = 0.757$ ($p < 0.001$) with MCD64A1 (2001–2022) and $\rho = 0.666$ ($p < 0.01$) with FireCCI51 (2001–2020), indicating that the fused results generally retained the interannual variation patterns of the two input products. The final burned area polygons were spatially overlaid with parameter datasets at a 30 m spatial scale, and the resulting burned area data were used as the burned area parameter (BA) in Equation (1).

2.2.2. Model Parameter Acquisition

Burned area data were obtained from two satellite remote sensing burned area products: FireCCI51 and MCD64A1. FireCCI51 and MCD64A1 were acquired through the GEE platform, where the required bands were composited monthly and batch-exported as monthly fire products, covering the periods from 2001 to 2020 and from 2001 to 2022, respectively. The basic information of the two burned-area products is summarized in Table 1. Land cover data were derived from the GLC_FCS30D global 30-m land-cover dynamic monitoring product with a fine classification system, accessed through the GEE platform. Annual land-cover maps from 2001 to 2022 were used in this study, with the corresponding GLC_FCS30D land-cover map applied for each year. The spatial resolution was 30 m. The dataset distinguishes five forest types: EBF, DBF, ENF, DNF, and MF. Annual forest-cover maps were spatially overlaid with the corresponding burned-area data to extract forest burned areas by forest type. No burned pixels classified as EBF or MF were identified during the study period. Therefore, subsequent emission estimates involved only DBF, ENF, and DNF. Aboveground biomass density data were obtained from the China Forest Aboveground Biomass Time-Series Dataset (CFATD), which has a spatial resolution of 30 m and covers the period from 2001 to 2022. Emission factors for CO_2, CO, and CH_4 were assigned according to forest type based on previous biomass-burning and forest fire emission studies, with additional consideration of parameter settings adopted in related studies from Northeast China [22–24]. Detailed parameter values are provided in Table 2.

Table 1. Characteristics of the burned-area products used in this study.

Dataset	Spatial Resolution	Temporal Resolution	Study Period
FireCCI51	250 m	Monthly	2001–2020
MCD64A1	500 m	Monthly	2001–2022

Table 2. Emission factors for different forest types ($g \cdot kg^{-1}$).

Forest Type	CO_2	CO	CH_4
DBF	1630	102	5.0
ENF	1514	118	6.0
DNF	1514	118	6.0

2.3. Spatial Autocorrelation Analysis

Counties were used as the basic spatial units of analysis in this study. Moran's I [25] was employed to examine the spatial autocorrelation characteristics of CO_2 emissions from forest fires in Heilongjiang Province. Global spatial autocorrelation was used to characterize

the overall spatial clustering pattern of CO_2 emissions from forest fires across the study area. Global Moran's I (I_G) is defined as follows:

$$I_G = \frac{n\sum_{i=1}^{n}\sum_{j=1}^{n} w_{ij}(x_i - \overline{x})(x_j - \overline{x})}{\left(\sum_{i=1}^{n}\sum_{j=1}^{n} w_{ij}\right)\sum_{i=1}^{n}(x_i - \overline{x})^2} \quad (6)$$

where I_G is Global Moran's I; n is the total number of counties in the study area; w_{ij} is the spatial weight between counties i and j; x_i and x_j are the CO_2 emissions from forest fires in counties i and j, respectively; and $\overline{x}$ is the mean CO_2 emissions from forest fires across all counties in the study area. The value of I_G ranges from −1 to 1. When $I_G > 0$, CO_2 emissions from forest fires exhibit positive spatial autocorrelation (i.e., spatial clustering); when $I_G < 0$, they exhibit negative spatial autocorrelation (i.e., spatial dispersion); and when I_G approaches 0, they are considered to be randomly distributed in space. Additionally, the presence of spatial autocorrelation suggests the need to further consider spatially explicit regression models, such as geographically and temporally weighted regression (GTWR), because global models such as ordinary least squares (OLS) may not adequately capture spatial heterogeneity in the relationships between emissions and their potential drivers.

I_G can only reflect the overall spatial pattern and is unable to identify the locations of local clusters and their spatial heterogeneity. Therefore, local spatial autocorrelation analysis was conducted using the Local Indicators of Spatial Association (LISA) [26] to reveal the spatial association characteristics between each county and its neighboring spatial units. Local Moran's I (I_L), a representative LISA statistic, is defined as follows:

$$I_L = \frac{n(x_i - \overline{x})\sum_{j=1}^{n} w_{ij}(x_j - \overline{x})}{\sum_{i=1}^{n}(x_i - \overline{x})^2} \quad (7)$$

where I_L is Local Moran's I; all other variables are the same as those defined in Equation (6). Following significance testing, spatial association patterns can be classified into four categories. High–High (H–H) clustering and Low–Low (L–L) clustering indicate positive local spatial autocorrelation, where spatial units with similar values tend to be spatially clustered. In contrast, High–Low (H–L) clustering and Low–High (L–H) clustering indicate negative local spatial autocorrelation, where spatial units with dissimilar values tend to be spatially adjacent.

2.4. Regression Models for Driving Factor Analysis

To investigate the driving factors of forest fire CO_2 emissions, three regression models, namely Ordinary Least Squares (OLS), Geographically Weighted Regression (GWR), and Geographically and Temporally Weighted Regression (GTWR), were employed for the analysis.

OLS was used to establish the global regression relationship between forest fire CO_2 emissions and the potential driving factors. The model is expressed as follows:

$$y_i = \beta_0 + \sum_{k=1}^{P} \beta_k x_{ik} + \varepsilon_i \quad (8)$$

where y_i represents the forest fire CO_2 emissions at sample point i; x_{ik} represents the observed value of the k-th independent variable at sample point i; β_0 is the intercept; β_k is the regression coefficient of the k-th independent variable; P is the number of independent variables; and ε_i is the random error term. The OLS model was implemented in R software (version 4.4.3; R Foundation for Statistical Computing, Vienna, Austria) using the lm()

function from the stats package. Based on the OLS model, the variance inflation factor (VIF) was used to assess multicollinearity among the independent variables, and significance tests were conducted to evaluate the statistical significance of the driving factors.

GWR incorporates spatial location into the regression model, allowing the regression coefficients to vary with spatial location and thereby characterizing the spatial heterogeneity in the relationships between the driving factors and forest fire CO_2 emissions. The model is expressed as follows [27]:

$$y_i = \beta_0(u_i, v_i) + \sum_{k=1}^{P} \beta_k(u_i, v_i) x_{ik} + \varepsilon_i \quad (9)$$

where (u_i,v_i) represents the spatial coordinates of sample point i; $\beta_0(u_i,v_i)$ is the local intercept at location i; and $\beta_k(u_i,v_i)$ is the local regression coefficient of the k-th independent variable at location i. The meanings of the other parameters are the same as those in the OLS model.

GTWR further incorporates the temporal dimension into GWR, allowing the regression coefficients to vary with spatial location and time, thereby reflecting the spatiotemporal differences in the effects of different driving factors on forest fire CO_2 emissions. The GTWR model is defined as follows [28]:

$$y_i = \beta_0(u_i, v_i, t_i) + \sum_{k=1}^{P} \beta_k(u_i, v_i, t_i) x_{ik} + \varepsilon_i \quad (10)$$

where y_i is the forest fire CO_2 emissions at sample point i; (u_i,v_i,t_i) denotes the spatiotemporal coordinates of sample point i, where u_i, v_i and t_i represent longitude, latitude, and time, respectively; $\beta_0(u_i,v_i,t_i)$ is the intercept term at sample point i; $\beta_k(u_i,v_i,t_i)$ is the local regression coefficient of the k-th independent variable at sample point i; P is the total number of independent variables; x_{ik} is the observed value of the k-th independent variable at sample point i, which may be either temporally varying or time-invariant; for time-invariant variables such as elevation, the value remains constant over time at a given spatial location; and ε_i is the random error term.

The 0.1° grid was used as the basic spatial analysis unit. GTWR constructs spatiotemporal distances from the spatial coordinates and temporal information of the observations to determine local weights. The relative scaling of spatial and temporal distances is controlled by a spatiotemporal distance ratio, which was determined through automatic optimization. A fixed-bandwidth kernel weighting scheme was employed, and the optimal bandwidth was selected based on AICc. The GWR and GTWR models were implemented in ArcGIS 10.8 (Esri, Redlands, CA, USA) using the GTWR Add-in (GTWR Beta 1.0), an extension for implementing the GTWR method proposed by Huang et al. [28].

The coefficient of determination (R^2), adjusted coefficient of determination (adjusted R^2), and corrected Akaike information criterion (AICc) were used as model evaluation metrics. Among them, R^2 and adjusted R^2 were used to assess the explanatory power of the model, with higher values indicating better model performance. AICc was used to evaluate the trade-off between model fit and model complexity, with lower values indicating better model performance.

2.5. Sources and Processing of Driving Factors

The driving factors of CO_2 emissions from forest fires included meteorological, topographic, vegetation, human activity, and socioeconomic factors (Table 3). Meteorological factors were obtained from the ERA5-Land reanalysis dataset provided by the European Centre for Medium-Range Weather Forecasts (ECMWF), including mean air temperature, total precipitation, 10 m wind speed, relative humidity, and potential evaporation, with a

monthly temporal resolution. Topographic factors were derived from the GEBCO (General Bathymetric Chart of the Oceans) global topographic dataset. Elevation data were extracted, and slope and aspect were subsequently calculated. Fractional vegetation cover data were obtained from the China 250 m Fractional Vegetation Cover Dataset provided by the National Tibetan Plateau Data Center. Based on the 1:250,000 National Fundamental Geographic Database provided by the National Geomatics Resource Catalog Service System, the Euclidean distances from the center of each grid cell to the nearest railway and road were calculated to construct two variables: distance to nearest railway (D_rail) and distance to nearest road (D_road). Population density data were obtained from the LandScan Global Population Distribution Dataset. Gross domestic product (GDP) data were derived from the global gridded GDP dataset developed by Kummu et al. [29] and were expressed in 2017 international dollars based on purchasing power parity (PPP). To ensure consistency in spatial scale, a 0.1° fishnet covering Heilongjiang Province was established as the common spatial analysis unit. Forest fire CO_2 emission data were aggregated from a spatial resolution of 30 m to the 0.1° grid, and all driving factors were spatially matched to the corresponding grids according to their spatial locations. For variables with multiple original spatial units within a grid, appropriate spatial aggregation was performed according to the characteristics of the data, thereby constructing a spatially matched dataset at the 0.1° grid scale. Subsequently, forest fire CO_2 emissions and all driving factors were standardized to eliminate the influence of differences in units and magnitudes.

Table 3. Data sources and characteristics of driving factors.

Data Type	Variable Name (Unit)	Abbreviation	Time Period	Spatial Resolution	Data Source
Meteorological factors	Mean Air Temperature (°C)	MAT	2001—2022	0.1°	ERA5-Land (https://cds.climate.copernicus.eu/datasets/reanalysis-era5-land-monthly-means) (accessed on 15 March 2026)
	Total Precipitation (mm)	TP	2001—2022	0.1°	
	Wind Speed ($m \cdot s^{-1}$)	WS	2001—2022	0.1°	
	Relative Humidity (%)	RH	2001—2022	0.1°	
	Potential Evaporation (m)	PEV	2001—2022	0.1°	
Topographic factors	Slope (°)	SLP	—	500 m	GEBCO (https://www.gebco.net/data-products/gridded-bathymetry-data) (accessed on 4 March 2026)
	Aspect (°)	ASP	—	500 m	
	Elevation (m)	ELE	—	500 m	
Vegetation factor	Fractional Vegetation Cover (%)	FVC	2001—2022	250 m	National Tibetan Plateau Data Center (http://data.tpdc.ac.cn) (accessed on 17 March 2026)
Human activity factors	Distance to Nearest Railway (m)	D_rail	—	0.1°	1:250,000 National Fundamental Geographic Database (https://mulu.tianditu.gov.cn) (accessed on 5 March 2026)
	Distance to Nearest Road (m)	D_road	—	0.1°	
Socioeconomic factors	Population Density (persons km^{-2})	PD	2001—2022	1 km	LandScan (https://landscan.ornl.gov/) (accessed on 14 March 2026)
	Gross Domestic Product (2017 international dollars, PPP)	GDP	2001—2022	1 km	(Kummu et al. [29])

3. Results

3.1. Temporal Patterns of Carbon Emissions from Forest Fires

3.1.1. Interannual Variability

From 2001 to 2022, CO_2, CO, and CH_4 emissions from forest fires in Heilongjiang Province showed overall downward trends (Figures 2 and S1). The downward trends were

statistically significant for all three gases (all $p < 0.001$), with linear rates of decline of 0.245 Tg yr^{-1}, 16.859 Gg yr^{-1}, and 0.810 Gg yr^{-1}, respectively. During the study period, the cumulative emissions of CO_2, CO, and CH_4 were approximately 72.95 Tg, 5171.73 Gg, and 246.54 Gg, respectively. The corresponding mean emissions per hectare of burned forest were 32.02, 2.27, and 0.108 Mg ha^{-1}, respectively. The three gases exhibited generally consistent interannual variation patterns and all reached their peak emissions in 2003, with CO_2, CO, and CH_4 emissions of approximately 13.05 Tg, 845.64 Gg, and 41.24 Gg, respectively; 2008 was another year with notably high emissions. In contrast, emissions of all three gases reached their lowest levels in 2012, subsequently rebounded and fluctuated, and then declined in each year from 2019 to 2022.

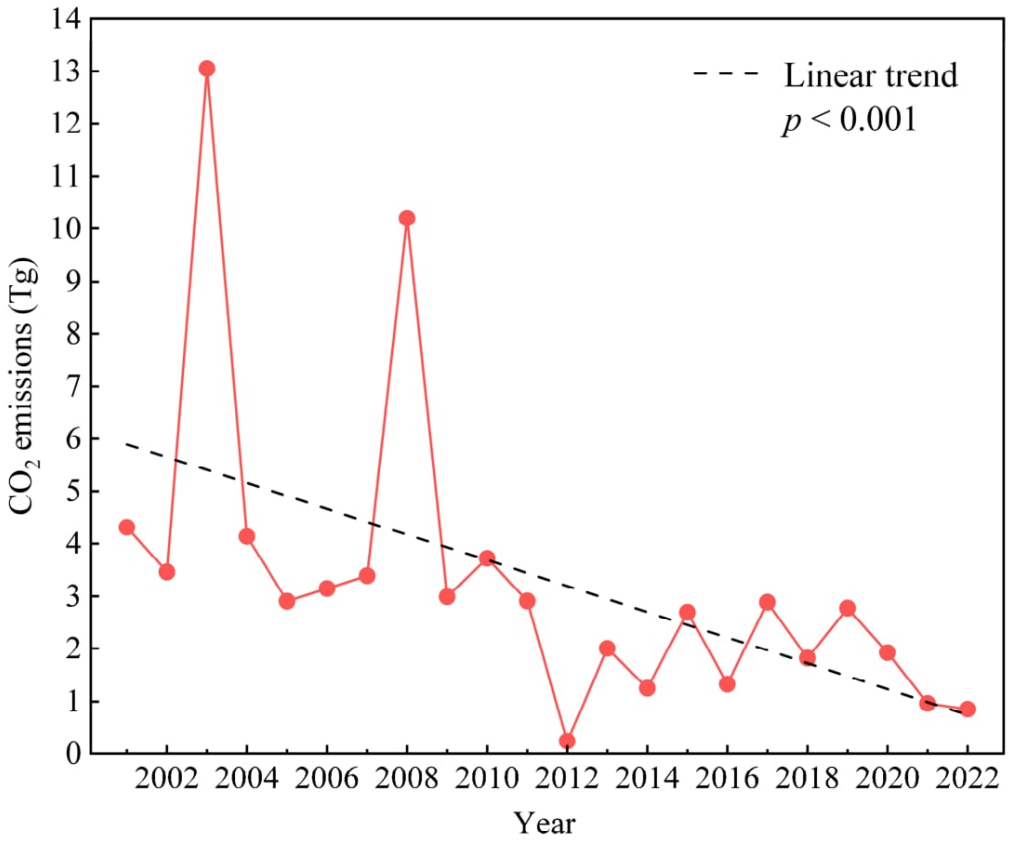


Figure 2. Interannual variations in CO_2 emissions from forest fires in Heilongjiang Province from 2001 to 2022. The black dashed line represents the linear trend fitted using ordinary least squares. The p value is derived from the two-sided Mann–Kendall trend test, a nonparametric test used to assess the presence of a monotonic increasing or decreasing trend in a time series. A p value < 0.05 indicates a statistically significant trend at the 0.05 significance level.

As shown in Figure 3, during the study period, CO_2 emissions from forest fires in Heilongjiang Province were distributed among three forest types: deciduous broadleaf forests (DBF), deciduous needleleaf forests (DNF), and evergreen needleleaf forests (ENF). In terms of burned area proportion (Figure 3b), DBF accounted for approximately 97.0% of the total burned area, far exceeding DNF (approximately 2.9%) and ENF (approximately 0.1%). In terms of interannual variation (Figure 3a), CO_2 emissions from forest fires in DBF consistently dominated across all years, and their interannual variation generally followed the overall trend of total forest fire CO_2 emissions in Heilongjiang Province, reaching a peak of approximately 12,537.70 Gg in 2003. During the study period, cumulative CO_2 emissions from forest fires in DBF were approximately 69,776.84 Gg, accounting for 95.6% of the total emissions. In contrast, cumulative CO_2 emissions from forest fires in DNF were

approximately 3084.29 Gg, accounting for 4.2% of the total emissions, with the annual peak likewise occurring in 2003 (approximately 504.99 Gg). ENF contributed only a small proportion of cumulative CO_2 emissions. On a per-hectare basis, mean CO_2 emissions were 31.71, 46.26, and 46.84 Mg CO_2 ha^{-1} of burned forest for DBF, DNF, and ENF, respectively.

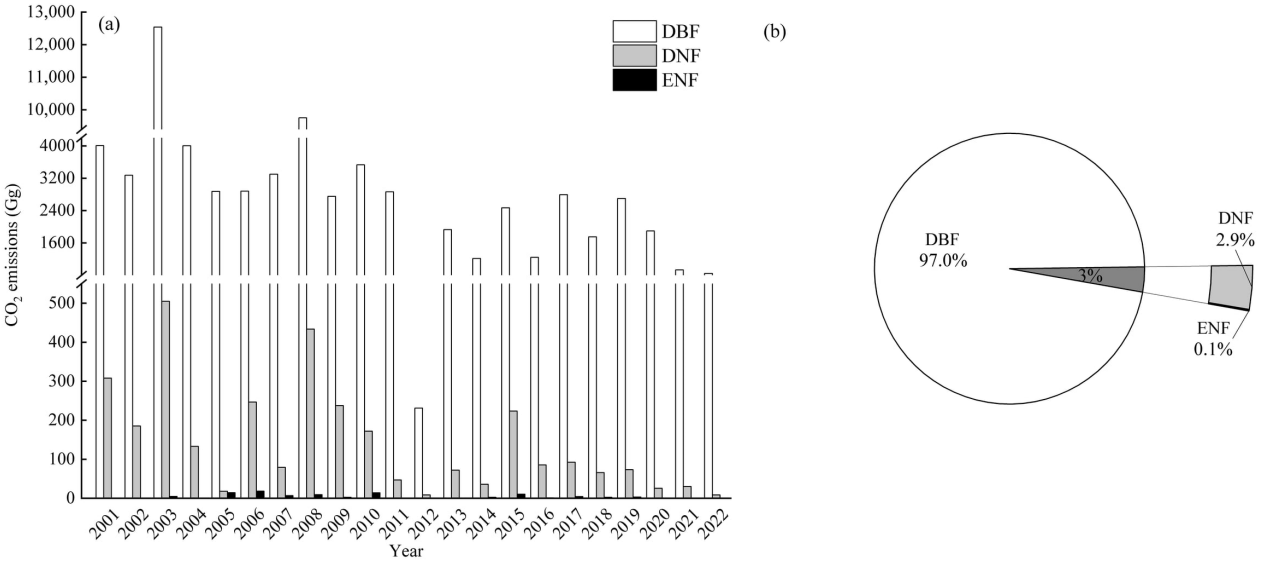


Figure 3. Annual CO_2 emissions from forest fires by forest type and proportions of burned area in Heilongjiang Province from 2001 to 2022. (**a**) Annual CO_2 emissions. (**b**) Proportions of burned area. DBF, Deciduous Broadleaf Forest; DNF, Deciduous Needleleaf Forest; ENF, Evergreen Needleleaf Forest.

3.1.2. Monthly Variability

From 2001 to 2022, CO_2, CO, and CH_4 emissions from forest fires in Heilongjiang Province exhibited pronounced seasonal variations at the monthly scale (Figures 4 and S2). The monthly cumulative emissions of the three gases showed generally consistent trends, with a distinct bimodal distribution characterized by higher emissions in spring and autumn and relatively lower emissions in summer and winter. Specifically, cumulative CO_2 emissions reached the highest level in March, at approximately 18.05 Tg, and formed another pronounced peak in October, at approximately 15.69 Tg; cumulative emissions were also relatively high in April and November, at approximately 13.37 Tg and 10.61 Tg, respectively. In contrast, CO_2 emissions were generally lower during summer (June–August) and winter (December, January, and February). The monthly variations in CO and CH_4 were generally consistent with those of CO_2.

3.2. Spatial Patterns of Carbon Emissions from Forest Fires

To facilitate the presentation of the overall spatial distribution pattern of multi-year mean emissions at the provincial scale, the original emission data at 30 m resolution were resampled to a 0.25° grid. From 2001 to 2022, the multi-year mean CO_2 emissions from forest fires in the forested areas of Heilongjiang Province exhibited pronounced spatial heterogeneity, with an overall pattern of decreasing emissions from north to south (Figure 5). High-emission areas were mainly concentrated in the northern part of the province, forming a continuous high-emission belt across the central and eastern sections of the Greater Khingan Mountains. Several high-emission patches were also distributed in the Lesser Khingan Mountains and their surrounding areas. In contrast, emission levels in the central region were generally low, with only a few areas exhibiting moderate-to-high emissions, whereas the southern region was dominated by low-emission areas.

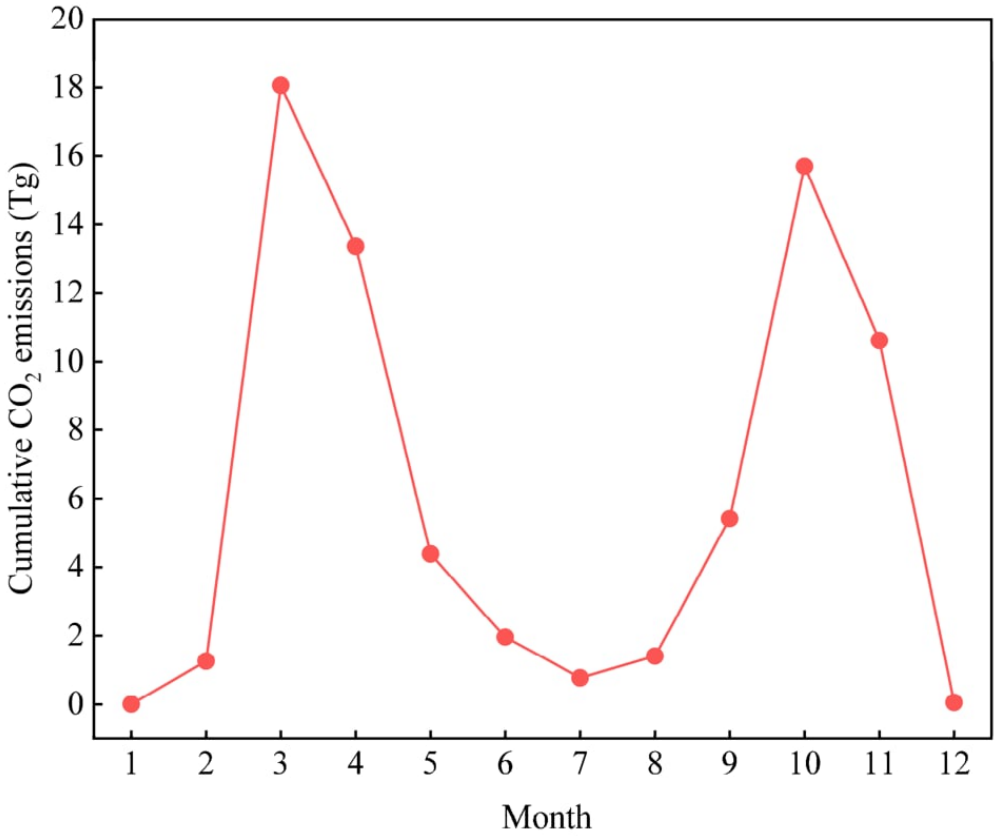


Figure 4. Monthly variations in CO_2 emissions from forest fires in Heilongjiang Province from 2001 to 2022.

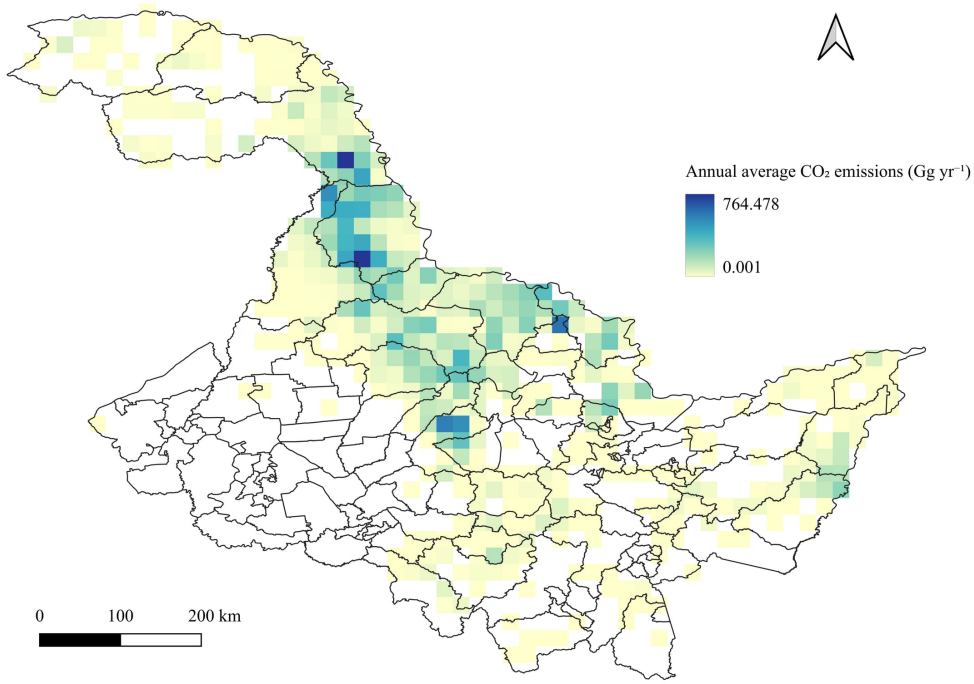


Figure 5. Spatial distribution of multi-year mean CO_2 emissions from forest fires in Heilongjiang Province from 2001 to 2022. The original emission data at 30 m resolution were resampled to a 0.25° grid to enhance visual clarity.

The results of Global Moran's *I* analysis showed that Moran's *I* values for forest fire CO_2 emissions in Heilongjiang Province remained positive throughout 2001–2022, indicating an

overall positive spatial autocorrelation during the study period (Table S1). Five representative years, selected at approximately five-year intervals, are presented in Table 4 to illustrate the temporal variation in spatial autocorrelation. Forest fire CO_2 emissions at the county level exhibited pronounced spatial clustering, with high-emission counties adjacent to other high-emission counties and low-emission counties adjacent to other low-emission counties. Among the five selected representative years, spatial autocorrelation was strongest in 2001 (Moran's $I = 0.295$), followed by 2011 and 2016, whereas relatively lower Moran's I values were observed in 2006 and 2021. The spatial autocorrelation in all representative years presented in Table 4 was statistically significant ($p < 0.001$), indicating significant positive spatial autocorrelation of forest fire CO_2 emissions in these years.

Table 4. Global spatial autocorrelation analysis of forest fire CO_2 emissions in selected representative years in Heilongjiang Province.

Year	Moran's *I*	*Z*-Score	*p*-Value
2001	0.295	5.807	<0.001
2006	0.067	7.396	<0.001
2011	0.213	4.128	<0.001
2016	0.168	9.002	<0.001
2021	0.066	4.245	<0.001

Figure 6 shows the local spatial autocorrelation (LISA) clustering patterns of forest fire CO_2 emissions in Heilongjiang Province. Pronounced spatial clustering characteristics were observed in all years. The clustering results were classified into three types: high–high (H–H), low–low (L–L), and low–high (L–H) clusters. From the perspective of spatial distribution, H–H clusters were mainly distributed in the northern part of the province, forming a belt-like clustering pattern extending from the Greater Khingan Mountains to the Heihe region. In 2006 and 2016, extensive and continuous H–H cluster belts were observed. Similar continuous distributions were also observed in 2001 and 2011, although their spatial extents were relatively smaller. In 2021, the H–H clusters contracted markedly and became localized in central counties. L–L clusters were mainly distributed in the Songnen Plain region of central-western Heilongjiang and occurred only in 2001 and 2011, with representative counties including Lindian County and Anda City. L–H clusters were sporadically distributed in the transitional zone between the northern forest region and the central plain, exhibiting weak spatial continuity. Overall, although the clustering types of individual counties varied among different years, the spatial pattern was characterized by the predominance of H–H clustering in the northern forest region and non-significant or L–L clustering in the Songnen Plain.

3.3. Analysis of the Driving Factors of Forest Fire CO_2 Emissions

To investigate the driving factors of forest fire CO_2 emissions, three models, namely OLS, GWR, and GTWR, were applied in this study. First, variable multicollinearity and significance tests were conducted based on the OLS model. The multicollinearity test results showed that the variance inflation factors (VIFs) for all independent variables were less than 5, indicating the absence of significant multicollinearity. The significance test results indicated that mean air temperature (MAT) and gross domestic product (GDP) did not reach statistical significance; therefore, the OLS significance test was used as an initial criterion for variable screening. Given that OLS is a global model, its significance results may not fully capture the spatial and temporal heterogeneity in the relationships between the driving factors and forest fire CO_2 emissions. Therefore, GTWR models with and without MAT and GDP were further compared. The results showed that including these two variables did not improve the overall model fit, and they were therefore not retained in the final GTWR model. After determining the final set of variables, the OLS,

GWR, and GTWR models were constructed using the selected variables, and their model fitting results are presented in Table 5. The results showed that the GTWR model achieved the best performance (R^2= 0.586; adjusted R^2 = 0.585), with the highest explanatory power and the lowest AICc value among the three models. Compared with the OLS and GWR models, the GTWR model explained approximately 58.5% of the variation in forest fire CO_2 emissions. Therefore, the GTWR model was subsequently applied to further analyze the driving factors of forest fire CO_2 emissions.

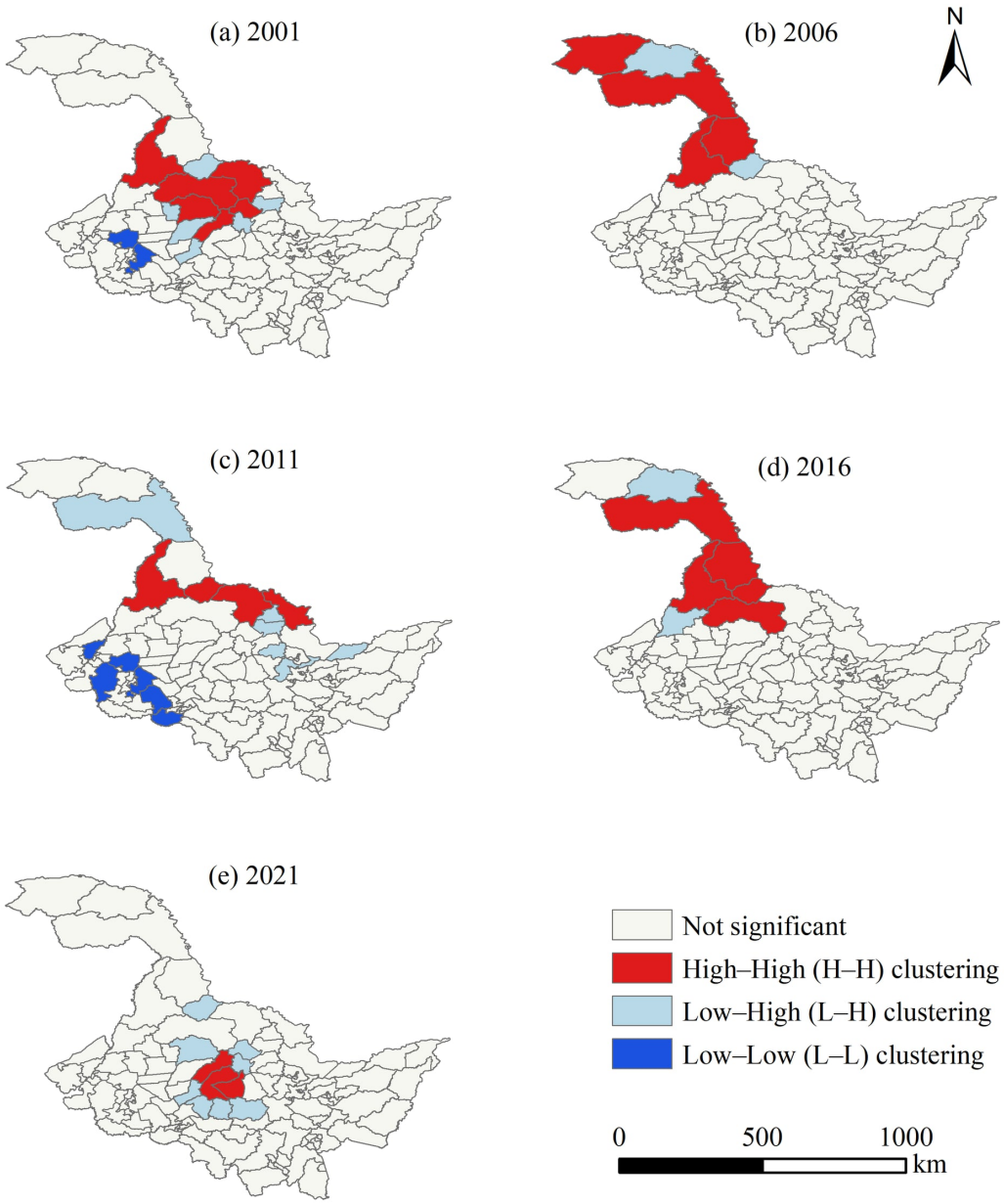


Figure 6. Local spatial autocorrelation (LISA) clustering patterns of forest fire CO_2 emissions in Heilongjiang Province. (**a**) 2001; (**b**) 2006; (**c**) 2011; (**d**) 2016; (**e**) 2021.

Table 5. Comparison of model fitting performance among different regression models.

Model	R^2	Adjusted R^2	AICc
OLS	0.410	0.408	10,879.55
GWR	0.528	0.525	10,002.80
GTWR	0.586	0.585	9561.61

Figure 7 illustrates the temporal evolution of the annual average regression coefficients of the driving factors in the GTWR model for forest fire CO_2 emissions in Heilongjiang Province from 2001 to 2022. Positive and negative coefficients indicate the direction of the influence of each factor on forest fire CO_2 emissions, whereas the coefficient magnitude reflects the strength of its effect. Among the vegetation factors, the regression coefficient of FVC remained consistently positive and had the largest coefficient values among all factors (0.23–0.68). The coefficient reached its peak in 2006, followed by a fluctuating downward trend, and showed a slight rebound after 2015. Among the human activity factors, the regression coefficients of D_rail and D_road were generally positive and exhibited fluctuating upward trends over time, with more pronounced increases after 2016, and the coefficients remained above 0.2 throughout most of the study period. In contrast, the regression coefficient of PD was relatively high and positive during the early study period, declined markedly thereafter, and remained at a relatively low level after 2013. Among the meteorological factors, the regression coefficients of WS and RH remained consistently negative and showed highly consistent temporal trends. Their negative effects became more pronounced during 2007–2010, after which the coefficients increased but remained negative. The regression coefficient of TP was also predominantly negative, although its absolute values were relatively small. The regression coefficient of PEV was generally positive, reaching relatively high levels during 2007–2011, declining thereafter, and increasing again after 2020. Among the topographic factors, the regression coefficient of ELE was generally negative, with its negative effects becoming more pronounced during 2008–2011 and 2018–2021. The regression coefficient of SLP was also predominantly negative, with relatively small fluctuations over time. The regression coefficient of ASP remained positive overall and fluctuated slightly around zero throughout the study period. In addition, the driving factors were ranked by relative importance based on the mean absolute values of their local GTWR regression coefficients (Table S2). FVC ranked first, with a mean absolute coefficient of 0.463, followed by PEV (0.268) and distance to the nearest railway (0.237).

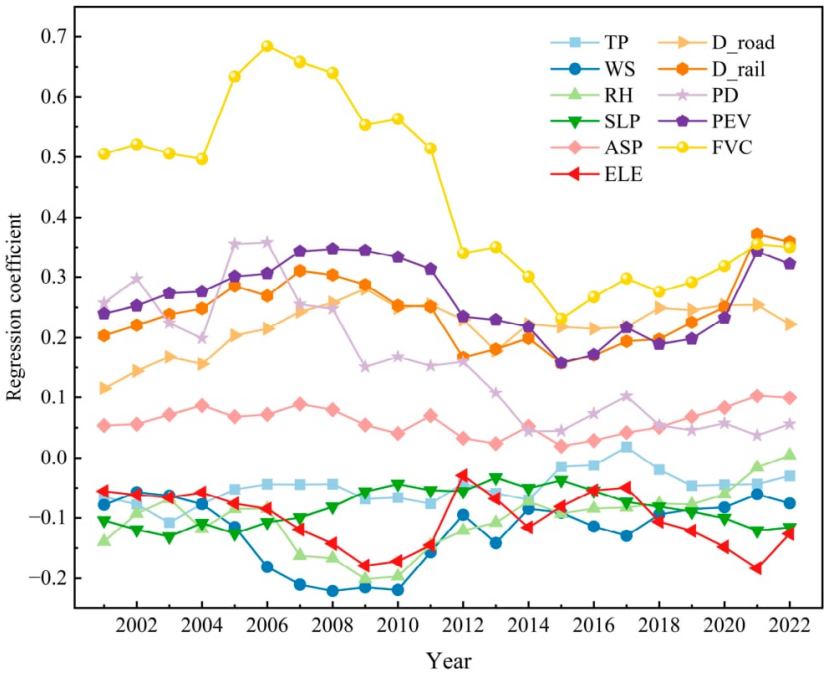


Figure 7. Temporal evolution of GTWR regression coefficients for forest fire CO_2 emissions in Heilongjiang Province from 2001 to 2022. TP, Total Precipitation; WS, Wind Speed; RH, Relative Humidity; PEV, Potential Evaporation; SLP, Slope; ASP, Aspect; ELE, Elevation; D_rail, Distance to Nearest Railway; D_road, Distance to Nearest Road; PD, Population Density; FVC, Fractional Vegetation Cover.

Figure 8 shows the spatial distribution of the GTWR regression coefficients for the driving factors of forest fire CO_2 emissions. The coefficients of FVC and PEV were positive, indicating positive relationships with forest fire CO_2 emissions, although the strength of these relationships varied spatially. The positive relationship for FVC was stronger in the northern forest regions, whereas that for PEV was more pronounced in parts of the central and southern regions. The coefficients of TP, WS, and RH were predominantly negative, but positive values occurred in some northern areas. WS and RH exhibited similar spatial patterns in their regression coefficients, with stronger negative relationships in parts of the northern forest regions and central Heilongjiang Province. The coefficients of D_rail and D_road were positive, with stronger positive relationships with CO_2 emissions in parts of the central and southern regions. The coefficients of PD were positive, with a stronger positive relationship with CO_2 emissions in the northern forest regions. Among the topographic factors, the coefficients of SLP and ELE were predominantly negative. The negative relationship for SLP was stronger in some northern areas, whereas ELE showed a stronger negative relationship mainly in central Heilongjiang Province. The coefficients of ASP were generally small, consisting mainly of values close to zero and small positive values.

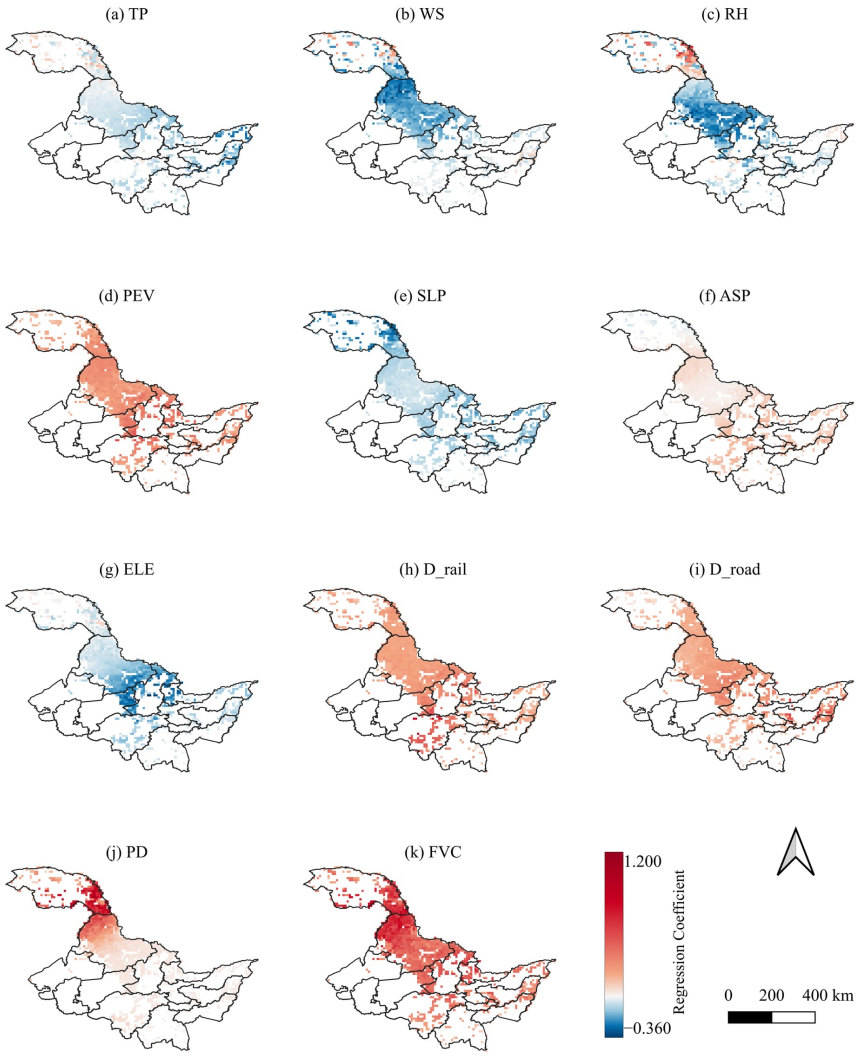


Figure 8. Spatial distribution of GTWR regression coefficients for the driving factors of forest fire CO_2 emissions in Heilongjiang Province from 2001 to 2022. (**a**) TP; (**b**) WS; (**c**) RH; (**d**) PEV; (**e**) SLP; (**f**) ASP; (**g**) ELE; (**h**) D_rail; (**i**) D_road; (**j**) PD; (**k**) FVC. Abbreviations are the same as those in Figure 7.

3.4. Comparison of Forest Fire CO_2 Emission Estimates

The forest fire CO_2 emissions estimated in this study for Heilongjiang Province from 2002 to 2022 were compared with those from the GFED5.1 dataset, as shown in Figure 9. The annual emission estimates from the two datasets were significantly positively correlated (Pearson $r = 0.707$, $p < 0.001$), and both showed 2003 and 2008 as years with notably high emissions. During the study period, the mean annual CO_2 emissions estimated in this study were approximately 3268.56 Gg, compared with approximately 2447.87 Gg from GFED5.1, and the estimates from this study were higher than those from GFED5.1 in most years. The estimates from this study were further compared with those reported in previous studies (Table 6). Li et al. [30] and Gong et al. [18] estimated the mean annual forest fire CO_2 emissions in Heilongjiang Province during 2001–2020 to be approximately 3914.77 Gg and 4700.00 Gg, respectively, both of which were higher than the corresponding estimate from this study for the same period (3556.89 Gg). The estimate from this study was closer to that reported by Li et al. [30].

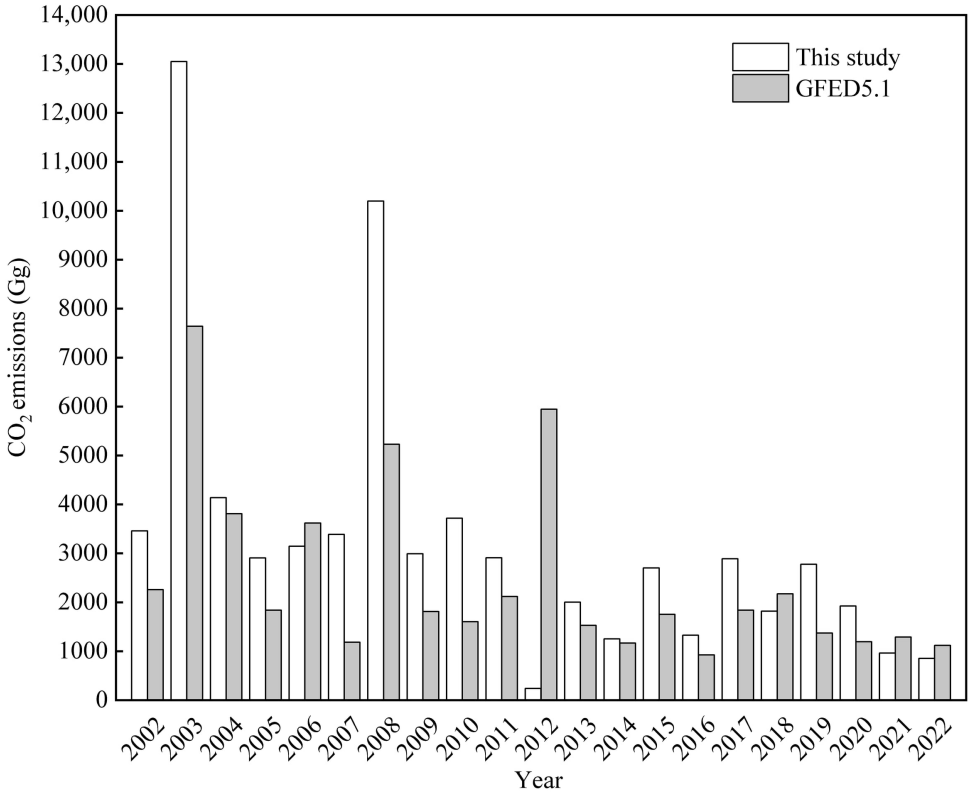


Figure 9. Comparison of forest fire CO_2 emissions between this study and GFED5.1 in Heilongjiang Province from 2002 to 2022.

Table 6. Comparison of forest fire CO_2 emission estimates in Heilongjiang Province from previous studies.

Reference	Study Period	Estimation Method	Spatial Scope	Mean Annual CO_2 Emissions (Gg yr^{-1})
Li et al. [30]	2001–2020	Emission factor method	Heilongjiang Province	3914.77
Gong et al. [18]	2001–2020	Bottom-up emission factor method	Heilongjiang Province	4700.00
This study	2001–2020	Emission factor method	Heilongjiang Province	3556.89

3.5. Uncertainty Estimation of Forest Fire Carbon Emissions

To assess the uncertainty in forest fire carbon emission estimates from 2001 to 2022, a Monte Carlo simulation was conducted by randomly sampling the major input parameters and propagating their uncertainties to the final emission estimates. The main sources of uncertainty were burned area (BA), aboveground biomass density (FL), combustion efficiency (CF), and emission factor (EF). Specifically, the uncertainty in BA was characterized based on the annual relative differences between the burned area estimates from FireCCI51 and MCD64A1. The uncertainties in FL and CF were determined based on relevant studies of the aboveground biomass density dataset [31] and the empirical relationship between dNBR and combustion efficiency [21]. The uncertainty in EF was determined based on literature-derived parameters and their standard deviations for different forest types [22–24]. On this basis, 100,000 Monte Carlo simulations were performed to estimate the annual emission ranges of CO_2, CO, and CH_4 with 95% confidence intervals (Table S3). From 2001 to 2022, the average range of the annual 95% confidence intervals for CO_2 emissions was 1723.57–5080.73 Gg, while the corresponding average ranges for CO and CH_4 emissions were 121.71–362.20 Gg and 5.83–17.33 Gg, respectively.

4. Discussion

4.1. Spatiotemporal Patterns of Forest Fire Carbon Emissions

At the interannual scale, forest fire carbon emissions in Heilongjiang Province showed an overall downward trend, although a few high-emission years still contributed substantially to cumulative emissions. This is consistent with Gong et al. [18], who reported an overall decline in forest fire CO_2 emissions in China during 2001–2022, while high emissions in Northeast China were mainly associated with sporadic extreme fire events. In this study, the high emissions in 2003 and 2008 coincided with relatively large burned areas, highlighting burned area as an important factor influencing carbon emissions. The subsequent rebound and fluctuations in emissions after 2012 were also broadly consistent with changes in burned area, and the reduction in burned area during 2019–2021 was accompanied by declining emissions. In addition, carbon emissions may reflect the combined effects of aboveground biomass density, combustion efficiency, and forest type. Therefore, regional forest fire management should continue to prioritize the prevention of large-scale fires and strengthen early fire detection and rapid response to limit fire spread and associated carbon emissions. Forest fire carbon emissions exhibited a bimodal seasonal pattern with peaks in spring and autumn, consistent with the seasonal patterns reported by Yin et al. [32] and Song et al. [33]. Elevated spring emissions may be associated with the exposure of surface fuels following snowmelt and dry, windy conditions that favor fire ignition and spread. Elevated autumn emissions may be associated with litter accumulation during the litterfall period and reduced air humidity, which increase surface fuel flammability. The spring and autumn emission peaks broadly coincide with the officially designated forest fire prevention periods in Heilongjiang Province. Therefore, ignition-source management, fire monitoring, and early warning should be strengthened during these two periods. DBF accounted for the largest share of burned area and contributed the most to cumulative forest fire CO_2 emissions. Zhang et al. [34] similarly found that DBF accounted for larger shares of both burned area and carbon emissions than DNF in Northeast China. However, CO_2 emissions per unit burned area were higher in DNF and ENF than in DBF in this study, indicating that contributions to total emissions did not correspond to emission levels per unit burned area across forest types. Within our estimation framework, emissions per unit burned area depend on aboveground biomass density, combustion efficiency, and the corresponding emission factors. Differences among forest types may therefore reflect the combined influence of these parameters.

The relatively high forest fire CO_2 emissions in the northern forest regions of Heilongjiang Province are consistent with the high-emission area identified in the Greater Khingan Mountains by a national-scale study [35]. This spatial difference may be related to the distribution of forest resources, fuel characteristics, and regional climatic conditions. The relatively high aboveground biomass and fuel loads in the northern forest regions may allow more fuel to burn under conditions conducive to fire spread, such as dry and windy weather, resulting in higher CO_2 emissions [36]. In contrast, agricultural land is more prevalent in the central and southern regions, where weaker forest continuity may limit forest fire spread. Furthermore, forest fire CO_2 emissions exhibited significant spatial clustering. Similarities in forest types, climate, and fuel conditions among neighboring areas, together with fire spread across spatial units, may jointly contribute to this clustering pattern [37].

4.2. Spatiotemporal Heterogeneity in the Driving Factors of Forest Fire CO_2 Emissions

Comparison of the OLS, GWR, and GTWR models showed that the GTWR model performed best (adjusted $R^2 = 0.585$). The GTWR results indicated spatiotemporal heterogeneity in the effects of the driving factors on forest fire CO_2 emissions: the strength of a given factor's effect varied across locations and years, and the direction of the effect also varied for some factors. It should be noted that the driving factors considered in the GTWR model did not explain all the variation in forest fire CO_2 emissions, which may be related to other influencing factors not incorporated into the model, such as fire management and suppression measures [38].

FVC was the most important influencing factor in this study in terms of relative importance. Its overall positive effect indicated that higher vegetation cover generally corresponded to higher forest fire CO_2 emissions. The positive effect of FVC was more pronounced in the northern forest regions, potentially reflecting the relatively abundant forest biomass and greater fuel continuity in these areas, which can facilitate fire spread and fuel consumption under conditions conducive to burning. Temporal variation in the strength of the FVC effect may reflect the combined influences of fuel accumulation, fire-related fuel consumption, and post-fire recovery. By consuming fuels and altering vegetation structure, fires may limit subsequent fire occurrence and spread; however, this constraint may weaken as vegetation recovers and fuels accumulate again [39].

PEV ranked second only to FVC in relative importance, and its overall positive effect on forest fire CO_2 emissions may be related to greater evaporative demand promoting fuel moisture loss. Fuel drying favors combustion and may increase the potential heat release from fires [40]. In contrast, TP and RH showed overall negative relationships with forest fire CO_2 emissions, potentially reflecting higher fuel moisture content and lower flammability under wetter conditions [41]. The relatively abundant fuels in the northern forest regions, together with meteorological influences on their dryness and flammability, may help explain the stronger effects of some meteorological factors in this region. WS showed an overall negative relationship with emissions. Shmuel and Heifetz [42] found that ignition probability decreased significantly when wind speed exceeded a certain threshold in their study, providing one possible explanation for the negative relationship observed here. Therefore, regional fire early warning should integrate fuel conditions with dynamic meteorological information to assess the likelihood of fire occurrence and spread.

Among the human activity factors, D_road and D_rail generally had positive coefficients, with stronger positive effects in parts of the central and southern regions. These relationships may reflect the influence of transport accessibility on fire detection and suppression response. Limited accessibility may constrain fuel management and fire suppression, increasing the likelihood of fires growing larger [43]. However, transport distances may

also reflect conditions such as remoteness and forest continuity. Among the socioeconomic factors, PD generally had positive coefficients, with stronger effects in the northern forest regions, potentially reflecting the combined influence of human ignition activities and relatively abundant fuels. Pozo et al. [44] also found regional differences in the relationships between socioeconomic factors, including PD, and wildfire activity. Therefore, regional fire prevention and control should prioritize early fire detection and suppression response in areas with limited transport accessibility and strengthen ignition-source patrols and management in priority areas based on population distribution and fuel conditions.

4.3. Uncertainty in Forest Fire Carbon Emission Estimates

This study employed Monte Carlo simulation to assess the uncertainty in forest fire carbon emission estimates. Estimation of forest fire carbon emissions involves multiple parameters, including burned area, aboveground biomass density, combustion efficiency, and emission factors. The data sources and parameter settings of these parameters may influence the estimation results. Burned area is one of the key factors affecting forest fire carbon emission estimates. Unlike most previous studies that rely on a single burned area product, this study integrated FireCCI51 and MCD64A1 to construct a long-term burned area dataset. However, differences in spatial resolution and fire detection algorithms among burned area products may still result in discrepancies in the identification of burned areas at the local scale [45]. The fused burned-area dataset has not been independently validated because suitable ground-reference data were unavailable. The effects of omission, commission, and boundary-location errors on emission estimates therefore require further assessment. The fixed dNBR threshold (0.2) adopted in this study was informed by previous burned-area mapping research in high-latitude boreal forest regions [20]. However, differences in forest type, pre-fire vegetation conditions, and environmental characteristics may affect its applicability in Heilongjiang Province. Unlike using a fixed combustion efficiency value, estimation based on an empirical dNBR relationship allows estimated combustion efficiency to vary spatially with dNBR. This empirical relationship was developed for forest ecosystems in a specific region, and its applicability across different forest types and fire conditions in Heilongjiang Province may be limited. Although CFATD provides high spatial resolution and a long time series, aboveground biomass density estimates derived from this dataset may still be affected by spatiotemporal mismatches among multisource remote sensing data, forest-type complexity, and model generalization ability [31]. In addition, this study did not account for carbon emissions from belowground biomass combustion, potentially underestimating emissions in areas where such combustion occurred. Emission factors are key parameters in forest fire emission estimation, and their values are jointly influenced by multiple factors, including fuel type, combustion phase, and combustion conditions [46]. Most currently available emission factors are derived from experimental measurements or regional empirical studies and may not fully represent actual emission characteristics under complex forest fire conditions, potentially introducing uncertainty into carbon emission estimates. Furthermore, the forest fire CO_2 emissions estimated in this study were higher than those from GFED5.1 in most years, potentially reflecting differences in burned-area data and fuel-consumption estimation methods. GFED5.1 estimates fuel consumption within a CASA-based biogeochemical modeling framework [47], which differs from the approach used in this study. Differences in forest classification and the selection of corresponding emission factors may also affect emission estimates for individual forest types, thereby contributing to differences in total regional CO_2 emissions. Continued updating of the emission estimation workflow requires supporting data for the corresponding years. Future studies could consider ESA CCI Biomass and other aboveground biomass products [48], or estimate aboveground biomass density using available local forest inventory data. Forest-

type information could be obtained from OpenGeoHub's Global Harmonized Land Cover (GHLC) product [49]. Alternatively, land-cover maps that distinguish forest types could be generated through remote sensing classification and independently validated. Updated inputs should be spatially aligned, and appropriate emission factors should be assigned according to forest type, enabling emission estimates to be extended to more recent years.

5. Conclusions

This study estimated forest fire CO_2, CO, and CH_4 emissions in Heilongjiang Province from 2001 to 2022 and analyzed their spatiotemporal patterns and the spatiotemporal heterogeneity in the relationships between driving factors and CO_2 emissions. During the study period, emissions of all three gases showed significant overall downward trends and a bimodal monthly pattern with spring and autumn peaks. Deciduous broadleaf forests contributed 95.6% of cumulative CO_2 emissions. Spatially, CO_2 emissions were generally higher in the north than in the south and exhibited significant spatial clustering. GTWR performed best among the models compared (adjusted $R^2 = 0.585$). The model results identified fractional vegetation cover as a main influencing factor and indicated that the relationships between driving factors and CO_2 emissions varied across space and over time. These findings can inform the development of regional forest fire management strategies. Ignition-source management, fire monitoring, and early warning should be strengthened in spring and autumn. In northern forest regions, vegetation, fuel conditions, and dynamic meteorological information should be integrated to identify priority monitoring areas, while areas with limited transport accessibility require greater attention to early fire detection and suppression response. Emission estimates remain subject to uncertainties in input data and empirical parameters. Future research should strengthen the collection of independent reference data and regional field observations to further validate and improve burned-area mapping and locally calibrate key parameters, including combustion efficiency and emission factors, thereby improving the reliability of regional forest fire carbon emission estimates.

Supplementary Materials: The following supporting information can be downloaded at: https://www.mdpi.com/article/10.3390/rs18223901/s1. Section S1: Statistical method (Mann–Kendall trend test); Table S1: Global spatial autocorrelation analysis results of CO_2 emissions from forest fires in Heilongjiang Province from 2001 to 2022; Table S2: Relative importance ranking of driving factors based on mean absolute local GTWR coefficients; Table S3: The uncertainty estimation of forest fire CO_2, CO, and CH_4 emissions in Heilongjiang Province from 2001 to 2022 (Gg); Figure S1: Interannual variations in CO and CH_4 emissions from forest fires in Heilongjiang Province from 2001 to 2022. (a) CO emissions; (b) CH_4 emissions. The black dashed lines represent the linear trends fitted using ordinary least squares. The p values are derived from the two-sided Mann–Kendall trend test, a nonparametric test used to assess the presence of a monotonic increasing or decreasing trend in a time series. A p value < 0.05 indicates a statistically significant trend at the 0.05 significance level; Figure S2: Monthly variations in CO and CH_4 emissions from forest fires in Heilongjiang Province from 2001 to 2022. (a) CO emissions; (b) CH_4 emissions.

Author Contributions: Conceptualization, H.C. and L.S.; methodology, H.C. and H.X.; formal analysis, Y.J.; investigation, Y.J. and H.X.; resources, H.C. and L.S.; data curation, Y.J. and L.L.; writing—original draft preparation, Y.J.; writing—review and editing, H.C., H.X. and L.S.; visualization, Y.J.; supervision, L.S.; project administration, L.S.; funding acquisition, L.S. All authors have read and agreed to the published version of the manuscript.

Funding: This research was funded by the Heilongjiang Province Double First-Class Discipline Collaborative Innovation Achievement Project (LJGXCG2022-007) and the Heilongjiang Excellent Youth Fund, China (YQ2024C032).

Data Availability Statement: The data presented in this study were derived from publicly available datasets. The FireCCI51, MCD64A1, GLC_FCS30D land-cover dataset, dNBR data, and CFATD dataset are available through the Google Earth Engine platform (https://earthengine.google.com/) (accessed on 23 February 2026). The meteorological factors used in this study were derived from the ERA5-Land reanalysis dataset provided by the European Centre for Medium-Range Weather Forecasts (ECMWF) (https://cds.climate.copernicus.eu/datasets/reanalysis-era5-land-monthly-means) (accessed on 15 March 2026). The GEBCO global topographic dataset is available through the official website (https://www.gebco.net/data-products/gridded-bathymetry-data) (accessed on 4 March 2026). The China 250 m Fractional Vegetation Cover Dataset is available from the National Tibetan Plateau Data Center (http://data.tpdc.ac.cn) (accessed on 17 March 2026). The 1:250,000 National Fundamental Geographic Database is available through the National Geomatics Resource Catalog Service System (https://mulu.tianditu.gov.cn) (accessed on 5 March 2026). The LandScan Global Population Distribution Dataset is available from its official website (https://landscan.ornl.gov/) (accessed on 14 March 2026). The annual CO_2 emission data generated in this study for 2001–2022 are publicly available on Zenodo at https://doi.org/10.5281/zenodo.22299941.

Acknowledgments: The authors sincerely appreciate the Ecosystem Big Data Research and Development Center of Northeast Forestry University for providing equipment/computing support.

Conflicts of Interest: The authors declare no conflicts of interest.

Abbreviations

The following abbreviations are used in this manuscript:

ASP	Aspect
DBF	Deciduous Broadleaf Forest
DNF	Deciduous Needleleaf Forest
dNBR	Differenced Normalized Burn Ratio
D_rail	Distance to Nearest Railway
D_road	Distance to Nearest Road
EBF	Evergreen Broadleaf Forest
ELE	Elevation
ENF	Evergreen Needleleaf Forest
FVC	Fractional Vegetation Cover
GDP	Gross Domestic Product
GEE	Google Earth Engine
GFED	Global Fire Emissions Database
GWR	Geographically Weighted Regression
GTWR	Geographically and Temporally Weighted Regression
MAT	Mean Air Temperature
MF	Mixed Forest
NBR	Normalized Burn Ratio
NF	Non-forest
OLS	Ordinary Least Squares
PD	Population Density
PEV	Potential Evaporation
RH	Relative Humidity
SLP	Slope
TP	Total Precipitation
WS	Wind Speed

References

1. Dye, A.W.; Houtman, R.M.; Gao, P.; Anderegg, W.R.L.; Fettig, C.J.; Hicke, J.A.; Kim, J.B.; Still, C.J.; Young, K.; Riley, K.L. Carbon, Climate, and Natural Disturbance: A Review of Mechanisms, Challenges, and Tools for Understanding Forest Carbon Stability in an Uncertain Future. *Carbon Balance Manag.* **2024**, *19*, 35. [CrossRef] [PubMed]
2. Liu, Y.; Shi, Y. Estimates of Global Forest Fire Carbon Emissions Using FY-3 Active Fires Product. *Atmosphere* **2023**, *14*, 1575. [CrossRef]
3. Singh, S. Forest Fire Emissions: A Contribution to Global Climate Change. *Front. For. Glob. Change* **2022**, *5*, 925480. [CrossRef]

4. Zheng, B.; Ciais, P.; Chevallier, F.; Chuvieco, E.; Chen, Y.; Yang, H. Increasing Forest Fire Emissions despite the Decline in Global Burned Area. *Sci. Adv.* **2021**, *7*, eabh2646. [CrossRef] [PubMed]
5. Zheng, B.; Ciais, P.; Chevallier, F.; Yang, H.; Canadell, J.G.; Chen, Y.; van der Velde, I.R.; Aben, I.; Chuvieco, E.; Davis, S.J.; et al. Record-High CO_2 Emissions from Boreal Fires in 2021. *Science* **2023**, *379*, 912–917. [CrossRef] [PubMed]
6. Byrne, B.; Liu, J.; Bowman, K.W.; Pascolini-Campbell, M.; Chatterjee, A.; Pandey, S.; Miyazaki, K.; van der Werf, G.R.; Wunch, D.; Wennberg, P.O.; et al. Carbon Emissions from the 2023 Canadian Wildfires. *Nature* **2024**, *633*, 835–839. [CrossRef] [PubMed]
7. Qu, G.; Shi, Y.; Yang, Y.; Wu, W.; Zhou, Z. Methods, Progress and Challenges in Global Monitoring of Carbon Emissions from Biomass Combustion. *Atmosphere* **2024**, *15*, 1247. [CrossRef]
8. van der Werf, G.R.; Randerson, J.T.; Giglio, L.; van Leeuwen, T.T.; Chen, Y.; Rogers, B.M.; Mu, M.; van Marle, M.J.E.; Morton, D.C.; Collatz, G.J.; et al. Global Fire Emissions Estimates during 1997–2016. *Earth Syst. Sci. Data* **2017**, *9*, 697–720. [CrossRef]
9. Seiler, W.; Crutzen, P.J. Estimates of Gross and Net Fluxes of Carbon between the Biosphere and the Atmosphere from Biomass Burning. *Clim. Change* **1980**, *2*, 207–247. [CrossRef]
10. Hu, H.; Wei, S.; Sun, L. Estimation of carbon emissions due to forest fire in Daxing'an Mountains from 1965 to 2010. *Chin. J. Plant Ecol.* **2012**, *36*, 629–644. [CrossRef]
11. Hu, H.; Wei, S.; Sun, L. Estimating carbon emissions from forest fires during 2001 to 2010 in Daxing'anling Mountain. *Acta Ecol. Sin.* **2012**, *32*, 5373–5386. [CrossRef]
12. Hu, H.; Luo, B.; Wei, S.; Sun, L.; Wei, S.; Wen, Z. Estimation of carbonaceous gases emission from forest fires in Xiao Xing'an Mountains of Northeast China in 1953–2011. *Chin. J. Appl. Ecol.* **2013**, *24*, 3065–3076. [CrossRef]
13. Pessôa, A.C.M.; Anderson, L.O.; Carvalho, N.S.; Campanharo, W.A.; Junior, C.H.L.S.; Rosan, T.M.; Reis, J.B.C.; Pereira, F.R.S.; Assis, M.; Jacon, A.D.; et al. Intercomparison of Burned Area Products and Its Implication for Carbon Emission Estimations in the Amazon. *Remote Sens.* **2020**, *12*, 3864. [CrossRef]
14. Xu, W.; He, H.S.; Hawbaker, T.J.; Zhu, Z.; Henne, P.D. Estimating Burn Severity and Carbon Emissions from a Historic Megafire in Boreal Forests of China. *Sci. Total Environ.* **2020**, *716*, 136534. [CrossRef] [PubMed]
15. Zhang, Y.; Qin, D.; Yuan, W.; Jia, B. Historical Trends of Forest Fires and Carbon Emissions in China from 1988 to 2012. *J. Geophys. Res.-Biogeosci.* **2016**, *121*, 2506–2517. [CrossRef]
16. van der Werf, G.R.; Randerson, J.T.; Giglio, L.; Collatz, G.J.; Mu, M.; Kasibhatla, P.S.; Morton, D.C.; DeFries, R.S.; Jin, Y.; van Leeuwen, T.T. Global Fire Emissions and the Contribution of Deforestation, Savanna, Forest, Agricultural, and Peat Fires (1997–2009). *Atmos. Chem. Phys.* **2010**, *10*, 11707–11735. [CrossRef]
17. Guo, W.; Fang, L.; Lin, J.; Luo, R.; Cao, X. Forest fire emissions and meteorological drivers in southwest China based on himawari-8/9 satellite observations. *Res. Environ. Sci.* **2026**, *39*, 25–35. [CrossRef]
18. Gong, X.; Liu, Z.; Tian, J.; Wang, Q.; Li, G.; An, Z.; Han, Y. Spatiotemporal Patterns and Drivers of Wildfire CO_2 Emissions in China from 2001 to 2022. *Atmos. Chem. Phys.* **2025**, *25*, 10379–10401. [CrossRef]
19. Tian, Y.; Wu, Z.; Cui, S.; Hong, W.; Wang, B.; Li, M. Assessing Wildfire Susceptibility and Spatial Patterns in Diverse Forest Ecosystems across China: An Integrated Geospatial Analysis. *J. Clean. Prod.* **2025**, *490*, 144800. [CrossRef]
20. Chen, D.; Hall, J.V.; Hoffman-Hall, A.; Shevade, V.; Argueta, F.; Liang, X.; Loboda, T. The Arctic Boreal Burned Area (ABBA) Product. *Geosci. Data J.* **2026**, *13*, e70060. [CrossRef]
21. Balde, B.; Vega-Garcia, C.; Gelabert, P.J.; Ameztegui, A.; Rodrigues, M. The Relationship between Fire Severity and Burning Efficiency for Estimating Wildfire Emissions in Mediterranean Forests. *J. For. Res.* **2023**, *34*, 1195–1206. [CrossRef]
22. Akagi, S.K.; Yokelson, R.J.; Wiedinmyer, C.; Alvarado, M.J.; Reid, J.S.; Karl, T.; Crounse, J.D.; Wennberg, P.O. Emission Factors for Open and Domestic Biomass Burning for Use in Atmospheric Models. *Atmos. Chem. Phys.* **2011**, *11*, 4039–4072. [CrossRef]
23. Wiedinmyer, C.; Akagi, S.K.; Yokelson, R.J.; Emmons, L.K.; Al-Saadi, J.A.; Orlando, J.J.; Soja, A.J. The Fire INventory from NCAR (FINN): A High Resolution Global Model to Estimate the Emissions from Open Burning. *Geosci. Model Dev.* **2011**, *4*, 625–641. [CrossRef]
24. Lv, Z.; Shi, Y.; Guo, D.; Zhu, Y.; Man, H.; Zhang, Y.; Zang, S. High-Resolution Daily Emission Inventory of Biomass Burning in the Amur-Heilong River Basin Based on MODIS Fire Radiative Energy Data. *Remote Sens.* **2022**, *14*, 4087. [CrossRef]
25. Moran, P.A.P. Notes on Continuous Stochastic Phenomena. *Biometrika* **1950**, *37*, 17–23. [CrossRef]
26. Anselin, L. Local Indicators of Spatial Association—LISA. *Geogr. Anal.* **1995**, *27*, 93–115. [CrossRef]
27. Brunsdon, C.; Fotheringham, A.S.; Charlton, M.E. Geographically Weighted Regression: A Method for Exploring Spatial Nonstationarity. *Geogr. Anal.* **1996**, *28*, 281–298. [CrossRef]
28. Huang, B.; Wu, B.; Barry, M. Geographically and Temporally Weighted Regression for Modeling Spatio-Temporal Variation in House Prices. *Int. J. Geogr. Inf. Sci.* **2010**, *24*, 383–401. [CrossRef]
29. Kummu, M.; Kosonen, M.; Masoumzadeh Sayyar, S. Downscaled Gridded Global Dataset for Gross Domestic Product (GDP) per Capita PPP over 1990–2022. *Sci. Data* **2025**, *12*, 178. [CrossRef] [PubMed]
30. Li, B.; Xu, Z.; Liu, B.; Zhang, Z.; Qiu, W.; Wang, W. Development of a Finer-Resolution Multi-Year Emission Inventory for Open Biomass Burning in Heilongjiang Province, China. *Sci. Rep.* **2024**, *14*, 29969. [CrossRef] [PubMed]

31. Cai, Y.; Zhu, P.; Li, X.; Liu, X.; Chen, Y.; Shen, Q.; Xu, X.; Zhang, H.; Nie, S.; Wang, C.; et al. Dynamics of China's Forest Carbon Storage: The First 30 m Annual Aboveground Biomass Mapping from 1985 to 2023. *Earth Syst. Sci. Data* **2025**, *17*, 6993–7018. [CrossRef]
32. Yin, L.; Du, P.; Zhang, M.; Liu, M.; Xu, T.; Song, Y. Estimation of Emissions from Biomass Burning in China (2003–2017) Based on MODIS Fire Radiative Energy Data. *Biogeosciences* **2019**, *16*, 1629–1640. [CrossRef]
33. Song, R.; Wang, T.; Han, J.; Xu, B.; Ma, D.; Zhang, M.; Li, S.; Zhuang, B.; Li, M.; Xie, M. Spatial and Temporal Variation of Air Pollutant Emissions from Forest Fires in China. *Atmos. Environ.* **2022**, *281*, 119156. [CrossRef]
34. Zhang, W.; Yang, Y.; Hu, C.; Zhang, L.; Hou, B.; Wang, W.; Li, Q.; Li, Y. NPP and Carbon Emissions under Forest Fire Disturbance in Southwest and Northeast China from 2001 to 2020. *Forests* **2023**, *14*, 999. [CrossRef]
35. Chen, A.; Tang, R.; Mao, J.; Yue, C.; Li, X.; Gao, M.; Shi, X.; Jin, M.; Ricciuto, D.; Rabin, S.; et al. Spatiotemporal Dynamics of Ecosystem Fires and Biomass Burning-Induced Carbon Emissions in China over the Past Two Decades. *Geogr. Sustain.* **2020**, *1*, 47–58. [CrossRef]
36. Fan, D.; Wang, M.; Liang, T.; He, H.; Zeng, Y.; Fu, B. Estimation and Trend Analysis of Carbon Emissions from Forest Fires in Mainland China from 2011 to 2021. *Ecol. Inform.* **2024**, *81*, 102572. [CrossRef]
37. Portier, J.; Gauthier, S.; Robitaille, A.; Bergeron, Y. Accounting for Spatial Autocorrelation Improves the Estimation of Climate, Physical Environment and Vegetation's Effects on Boreal Forest's Burn Rates. *Landsc. Ecol.* **2018**, *33*, 19–34. [CrossRef] [PubMed]
38. Phillips, C.A.; Rogers, B.M.; Elder, M.; Cooperdock, S.; Moubarak, M.; Randerson, J.T.; Frumhoff, P.C. Escalating Carbon Emissions from North American Boreal Forest Wildfires and the Climate Mitigation Potential of Fire Management. *Sci. Adv.* **2022**, *8*, eabl7161. [CrossRef] [PubMed]
39. Parks, S.A.; Miller, C.; Holsinger, L.M.; Baggett, L.S.; Bird, B.J. Wildland Fire Limits Subsequent Fire Occurrence. *Int. J. Wildland Fire* **2016**, *25*, 182–190. [CrossRef]
40. Goodwin, M.J.; Zald, H.S.J.; North, M.P.; Hurteau, M.D. Climate-Driven Tree Mortality and Fuel Aridity Increase Wildfire's Potential Heat Flux. *Geophys. Res. Lett.* **2021**, *48*, e2021GL094954. [CrossRef]
41. Luo, K.; Quan, X.; He, B.; Yebra, M. Effects of Live Fuel Moisture Content on Wildfire Occurrence in Fire-Prone Regions over Southwest China. *Forests* **2019**, *10*, 887. [CrossRef]
42. Shmuel, A.; Heifetz, E. Empirical Evidence of Reduced Wildfire Ignition Risk in the Presence of Strong Winds. *Fire* **2023**, *6*, 338. [CrossRef]
43. Leonard, B.; Plantinga, A.J.; Wibbenmeyer, M. Stranded Land Constrains Public Land Management and Contributes to Larger Fires. *Environ. Res. Lett.* **2021**, *16*, 114014. [CrossRef]
44. Pozo, R.A.; Galleguillos, M.; Gonzalez, M.E.; Vasquez, F.; Arriagada, R. Assessing the Socio-Economic and Land-Cover Drivers of Wildfire Activity and Its Spatiotemporal Distribution in South-Central Chile. *Sci. Total Environ.* **2022**, *810*, 152002. [CrossRef] [PubMed]
45. Giglio, L.; Boschetti, L.; Roy, D.P.; Humber, M.L.; Justice, C.O. The Collection 6 MODIS Burned Area Mapping Algorithm and Product. *Remote Sens. Environ.* **2018**, *217*, 72–85. [CrossRef] [PubMed]
46. Urbanski, S. Wildland Fire Emissions, Carbon, and Climate: Emission Factors. *For. Ecol. Manag.* **2014**, *317*, 51–60. [CrossRef]
47. Van Der Werf, G.R.; Randerson, J.T.; Van Wees, D.; Chen, Y.; Giglio, L.; Hall, J.; Vernooij, R.; Mu, M.; Binte Shahid, S.; Barsanti, K.C.; et al. Landscape Fire Emissions from the 5th Version of the Global Fire Emissions Database (GFED5). *Sci. Data* **2025**, *12*, 1870. [CrossRef] [PubMed]
48. Santoro, M.; Cartus, O.; Quegan, S.; Kay, H.; Lucas, R.M.; Araza, A.; Herold, M.; Labrière, N.; Chave, J.; Rosenqvist, Å.; et al. Design and Performance of the Climate Change Initiative Biomass Global Retrieval Algorithm. *Sci. Remote Sens.* **2024**, *10*, 100169. [CrossRef]
49. Moreno, M.; Parente, L.; Hein, L.; Bonannella, C.; Xu, Q.; Isik, M.S.; Wibisana, M.I.; Piccoli, M.; Hengl, T. GHLC: Global Harmonized Land Cover Datasets for 2020–2024 at 10 m and 30 m Resolution Based on a Rule-Based Ensemble Approach. *EGUsphere* **2026**, *preprint*. [CrossRef]

Disclaimer/Publisher's Note: The statements, opinions and data contained in all publications are solely those of the individual author(s) and contributor(s) and not of MDPI and/or the editor(s). MDPI and/or the editor(s) disclaim responsibility for any injury to people or property resulting from any ideas, methods, instructions or products referred to in the content.